

High as-cast strength die-cast AlSi9Cu2Mg alloy prepared by nanoparticle strengthening with industrially acceptable ductility

Xixi Dong^{*}, Hamza Youssef, Xiangzhen Zhu, Yijie Zhang, Shihao Wang, Shouxun Ji^{*}
Brunel Centre for Advanced Solidification Technology (BCAST), Brunel University London,
Uxbridge Middlesex UB8 3PH, United Kingdom

^{*}Corresponding author: Tel: +44 1895 266663; Fax: +44 1895 269758

E-mail address: xixi.dong@brunel.ac.uk, shouxun.ji@brunel.ac.uk

ABSTRACT

High strength die-cast AlSi9Cu2Mg alloy strengthened by the addition of titanium diboride nanoparticles under as-cast condition was achieved with industrially acceptable ductility. The main intermetallic compounds in the die-cast AlSi9Cu2Mg alloy were identified as θ -Al₂Cu and Q-Al₅Cu₂Mg₈Si₆ phases. The Fe-rich compound formed in the alloy with a high Mn/Fe ratio of 3:1 was determined as the BCC structured α -Al₁₅(Fe,Mn)₃Si₂ phase with a lattice parameter of $a = 1.2702$ nm, and the Fe-rich compound had highly faceted morphology with {110} surface termination. The primary α -Al phase in the die-cast AlSi9Cu2Mg alloy was refined by 65 % from 18.1 μm to 6.4 μm , after adding 3.0wt.% titanium diboride nanoparticles. The titanium diboride nanoparticles in the alloy showed coherent interface with the Al matrix, with the (11-1) lattice face of Al parallel to the (0001) lattice face of titanium diboride. The as-cast AlSi9Cu2Mg alloy containing 3.0wt.% titanium diboride nanoparticles exhibited the high yield strength of 233 ± 3 MPa and the tensile strength of 398 ± 7 MPa, as well as the industrially acceptable good elongation of 4.8 ± 0.7 %, showing 23 % improvement in the as-cast yield strength over the alloy without reinforcement particles. The strengthening by nanoparticles with coherent interface (~ 32 MPa) was higher than that by refining the primary α -Al phase (~ 10 MPa). The addition of titanium diboride nanoparticles also affected the fracture because cracks were initiated from the eutectic Si phase in the alloy without particles, but from the Q and Fe-rich compounds in the alloy with 3wt.% titanium diboride nanoparticles.

Keywords: Aluminium alloys; Microstructure; Mechanical properties; Intermetallic compounds; Interface.

1. Introduction

High pressure die casting (HPDC) is a highly efficient precision casting method for the massive production of lightweight aluminium or magnesium alloy parts in automobile, aerospace and other transport manufacturing industries. In HPDC, the Al or Mg alloy melts are injected into steel die cavities through a shot sleeve [1–5]. In industry, most of the HPDC parts are fabricated by traditional non-vacuum methods and not suitable for further strengthening by solution and ageing heat treatment due to the blistering in the HPDC parts after solution heat treatment [6–8]. Although the recently developed vacuum-assisted HPDC is a way to produce heat treatable die-castings [9–11], extra time and energy costs are associated in the production. Therefore, most of the HPDC parts are preferred to be used in as-cast state.

Aluminium alloys are more widely applied than Mg alloys due to the good corrosion resistance, and the urgent requirements of lightweight in transport. Unfortunately, the as-cast yield strength (YS) of the generally applied die-cast Al alloys are always in the range of 90–170 MPa, of which the popular die-cast A380 Al alloy offers ~150 MPa [12,13]. Different investigations were tried to improve the as-cast YS of die-cast Al alloys via the regular alloy composition optimization, but the enhancements were not so significant considering that, in satisfaction of industrially acceptable ductility of 4 % in the standard tensile samples, the YS of die-cast Al alloys are still below 190 MPa [14–17]. Therefore, particle strengthening is a possible solution to achieve high strength for die-cast Al alloys under as-cast condition because of the strengthening effectiveness.

Various ceramic particles such as titanium diboride, alumina, silicon carbide, silicon nitride and titanium carbide were reported [18–26] for the reinforcement of gravity cast Al alloys or wrought Al alloys, but studies on the particle strengthening of die-cast Al alloys are quite insufficient [27]. The titanium diboride is a special particle that could be synthesized at nanoscale in Al melt by in-situ chemical reaction [28], and the titanium diboride nanoparticles are more wet-able with Al alloy melts. Therefore, the in-situ synthesised titanium diboride nanoparticle is possibly an ideal choice for the strengthening of die-cast Al alloys.

In this work, the titanium diboride nanoparticles were added into the AlSi9Cu2Mg die-cast alloy melt for studying the high strength die-cast Al alloys under as-cast condition. The microstructure especially intermetallic compounds, mechanical properties, strengthening and

fracture mechanisms of the alloy were investigated to understand the effect of titanium diboride nanoparticles in the HPDC aluminium alloys.

2. Experiments

2.1. Preparation of alloy melts

Table 1 shows the chemical contents of the AlSi9Cu2Mg die-cast alloys with different levels of titanium diboride (TiB₂) nanoparticles. One electric resistance furnace was applied for melting the die-cast alloys at the temperature of 760 °C. 1.5 wt.% and 3.0 wt.% TiB₂ nanoparticles were added into the alloy melts via adding the in-situ synthesised Al and TiB₂ master alloy containing 10 wt.% TiB₂. The preparation and microstructure of the Al and TiB₂ master alloy is described in 3.1.1. Argon was injected into the alloy melt through an impeller rotating machine at 400 rpm for degassing. The degassing time was set for 6 min. The final density index was controlled at a level of <0.3%.

Table 1. Contents of elements in the experimental alloys (wt.%).

Nanoparticle	Si	Mg	Cu	Mn	Fe	Ti	B	Sr	Al
0	9.02	0.47	1.98	0.55	0.18	0.12	0.001	0.019	Bal.
1.5	8.98	0.48	1.97	0.56	0.17	1.16	0.472	0.019	Bal.
3.0	9.03	0.48	1.99	0.55	0.18	2.20	0.938	0.020	Bal.

2.2. HPDC and tensile tests

A steel die was machined and fit on a 450-tonne cold chamber HPDC machine to make round mechanical testing bars with the gauge diameter of $\phi 6.35$ mm and the gauge length of 50 mm. During HPDC. The die was preheated at 220 °C and the melts were poured at 700 °C. The tensile properties of the as-cast bars were tested at ambient temperature using an Instron tensile machine. During tensile tests, the extension speed was controlled at 1 mm/min. A minimum of sixteen bars were tested for each condition, and the average values were applied as the final tensile performance.

2.3. Microstructure analysis

Scanning electron microscope (SEM) and transmission electron microscopy (TEM) were applied for the microstructure analysis of the die-cast AlSi9Cu2Mg alloys. Energy dispersive X-ray spectroscopy (EDS) under SEM was used for composition analysis, and

electron backscatter diffraction (EBSD) was applied for the analysis of grain size. Standard polishing and vibration polishing were used for the fabrication of SEM and EBSD samples, respectively, and ion polishing was applied to obtain TEM samples. SEM and TEM characterization were performed under 20 kV and 200 kV, separately. Bright-field and high-resolution TEM (HRTEM) images as well as select area diffraction patterns (SADP) were obtained under high magnification TEM observation. X-ray diffraction (XRD) analysis was conducted on a D8 X-ray diffractometer in the 2 Theta range from 20° to 80°.

3. Results

3.1. Microstructure

3.1.1. Al and TiB₂master alloy

The Al and TiB₂master alloy containing 10 wt.% TiB₂nanoparticles was prepared via the in-situ chemical reaction of potassium tetrafluoroborate and potassium hexafluorotitanate salts in the 855 °C pure Al melt [28]. The TiB₂nanoparticles were the chemical reaction products, and the reacted melt was poured into the ingots of Al and 10 wt.% TiB₂master alloy. The microstructure of the Al and 10 wt.% TiB₂master alloy was observed under SEM, as shown in Fig. 1a, and numerous TiB₂nanoparticles were found distributing in the alloy. The in-situ generated TiB₂nanoparticle shows the faceted shape under the high magnification TEM observation, as shown in Fig. 1b, which conforms with the previous works [29,30]. The SADP result in Fig. 1c and the HRTEM result in Fig. 1d confirms that the nanoparticle shown in Fig. 1b is TiB₂. The in-situ formed TiB₂nanoparticles were well characterized ranging between 0 and 450 nm with the mean size of approximately 100 nm [30], which are in good agreement with the present observations.

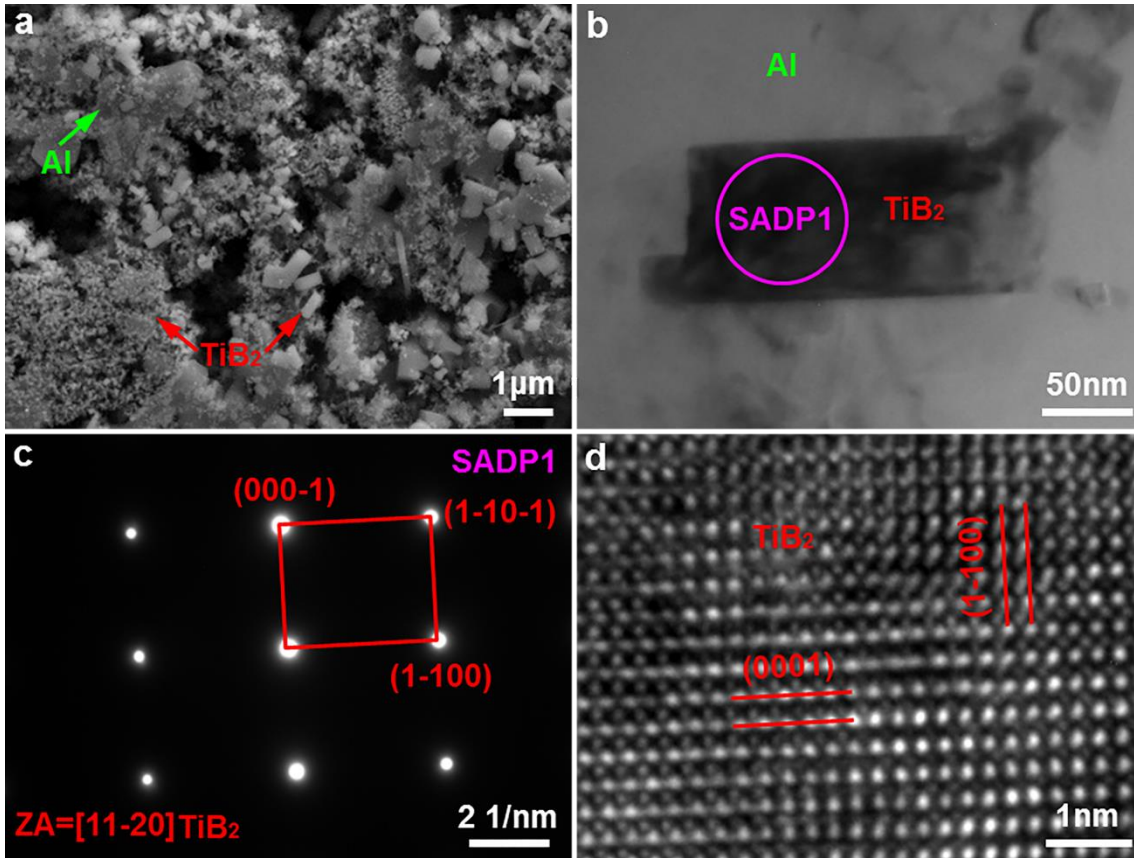


Fig. 1. Microstructure of the prepared Al and TiB₂ master alloy. (a) SEM morphology, (b) microstructure of the TiB₂ nanoparticle observed under TEM, (c) diffraction result and (d) high resolution micrograph of the TiB₂ shown in (b).

3.1.2. Die-cast AlSi9Cu2Mg alloy

3.1.2.1. Theoretical analysis

The AlSi9Mg0.5 alloy was reported as a high-performance cast Al alloy with excellent ductility and corrosion resistance, and the β -Mg₂Si phase was the main compound in the alloy for strengthening [8]. Unfortunately, the AlSi9Mg0.5 alloy is not excellent for elevated applications due to the lower stability and easier coarsening of the Mg₂Si precipitates. The addition of Cu can enable the AlSi9Mg0.5 alloy to be used at elevated temperatures, via the formation of Q and θ precipitates with higher thermal stability. Fig. 2 presents the evolution of different compounds in the AlSi9Mg0.5Cu alloy with Cu contents, via the theoretical calculation conducted on the thermodynamic software Pandat. The volume fraction of the β compound decreases with increasing the Cu content and disappears at ~1.0wt.% Cu. With the increase of Cu content, the volume fraction of Q compound increases obviously up to ~1.0wt.% Cu, and the volume fraction of θ compound increases continuously. The total

volume fraction of β , Q and θ compounds increases continuously with increasing the Cu contents, which indicates the capability of continuous compound strengthening of the alloy. However, too much addition of Cu will increase the hot-tearing tendency of the alloy. The intention of present addition of 2.0wt.% Cu is to eliminate the formation of β compound and to achieve a desirable strengthening effect without significantly worsening the hot-tearing tendency of the alloy after adding TiB₂ nanoparticles.

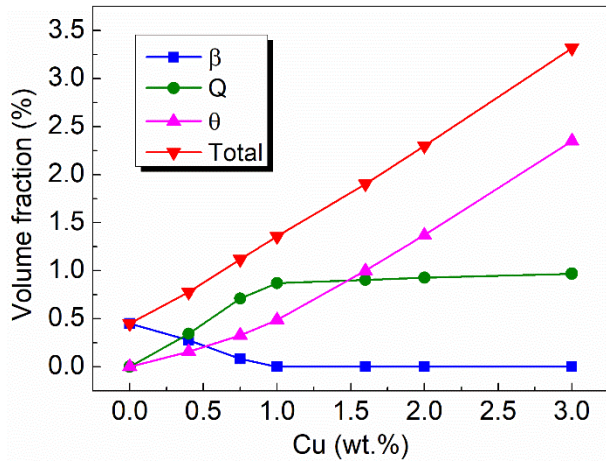


Fig. 2. Theoretical analysis of the evolution of different compounds in the AlSi9Mg0.5Cu alloy with Cu content via the thermodynamic calculation.

3.1.2.2. SEM morphology

Fig. 3 shows the microstructure of the as-cast AlSi9Cu2Mg alloy without the addition of TiB₂ nanoparticles, under backscattered electron SEM observation. Fig. 3a presents the low magnification morphology of the die-cast alloy, and α -Al phases with two different grain sizes were observed, i.e., the larger primary α_1 -Al phase and the finer primary α_2 -Al phase, which was due to the difference of cooling rate in shot sleeve and steel die. The eutectic silicon phase and the primary α -Fe₁ compound were also observed in Fig. 3a. The θ , Q, primary α -Fe₁ and secondary α -Fe₂ compounds were observed in the alloy, as shown in Fig. 3b-d. The θ and Q compounds located at α -Al boundaries, while the α -Fe₁ and α -Fe₂ compounds presented both at the α -Al boundaries and within the α -Al grains. The calculation conducted on the thermodynamic software Pandat showed that the α -Fe compound formed before the formation of α -Al phase, which provides the thermodynamic base for the presence of α -Fe compound in the α -Al grains. Yang et al. [31] also reported the presence of the early formed α -Fe compound in the α -Al grains of AlMg5.3Si2.4Fe1.0 (in wt.%) die-cast alloy. In addition, the θ compound is concentrated with Al and Cu, and the Q

compound is concentrated with Al, Si, Cu and Mg, while the two α -Fe compounds are concentrated with Al, Si, Mn and Fe, according to the EDS test patterns listed in Fig. 1S in the supplementary material.

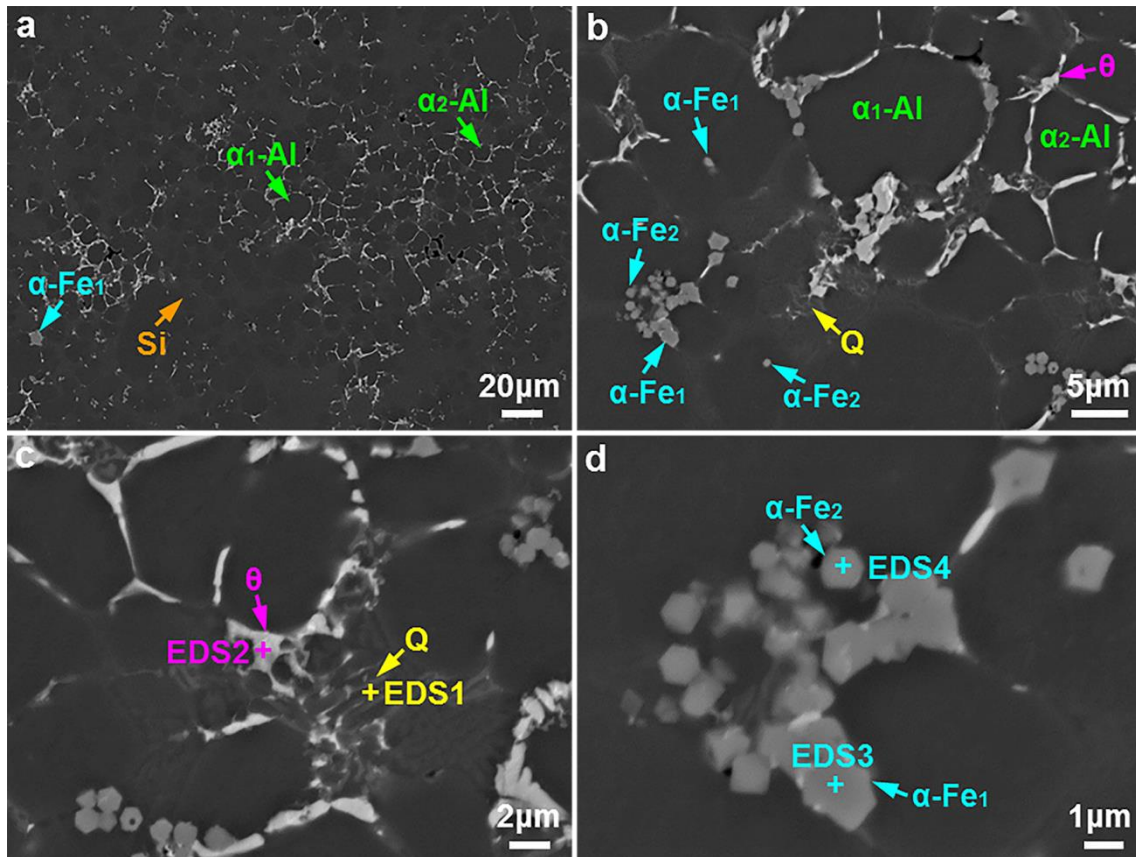


Fig. 3. SEM morphology of the as-cast AlSi9Cu2Mg alloy. (a) Micrograph of α -Al and silicon phases. (b) Distribution of the intermetallic compounds. (c) High magnification observation of θ and Q compounds. (d) High magnification observation of α -Fe compound.

3.1.2.3. TEM confirmation of compounds

TEM analysis was performed to confirm the three kinds of compounds observed under SEM for the as-cast AlSi9Cu2Mg alloy. Fig. 4a presents the shape of θ compound under TEM, and the SADP in Fig. 4b verifies that the θ compound is the body centred tetragonal Al_2Cu . Fig. 4c shows the shape of Q compound under TEM, and the SADP in Fig. 4d identifies that the Q compound is the hexagonal close packed $\text{Al}_5\text{Cu}_2\text{Mg}_8\text{Si}_6$. Fig. 4e presents the shape of α -Fe compound under TEM. The SADP in Fig. 4f confirms that the α -Fe compound is the body centred cubic $\text{Al}_{15}(\text{Fe},\text{Mn})_3\text{Si}_2$, and the α -Fe compound has faceted shape with the termination of $\{110\}$ planes.

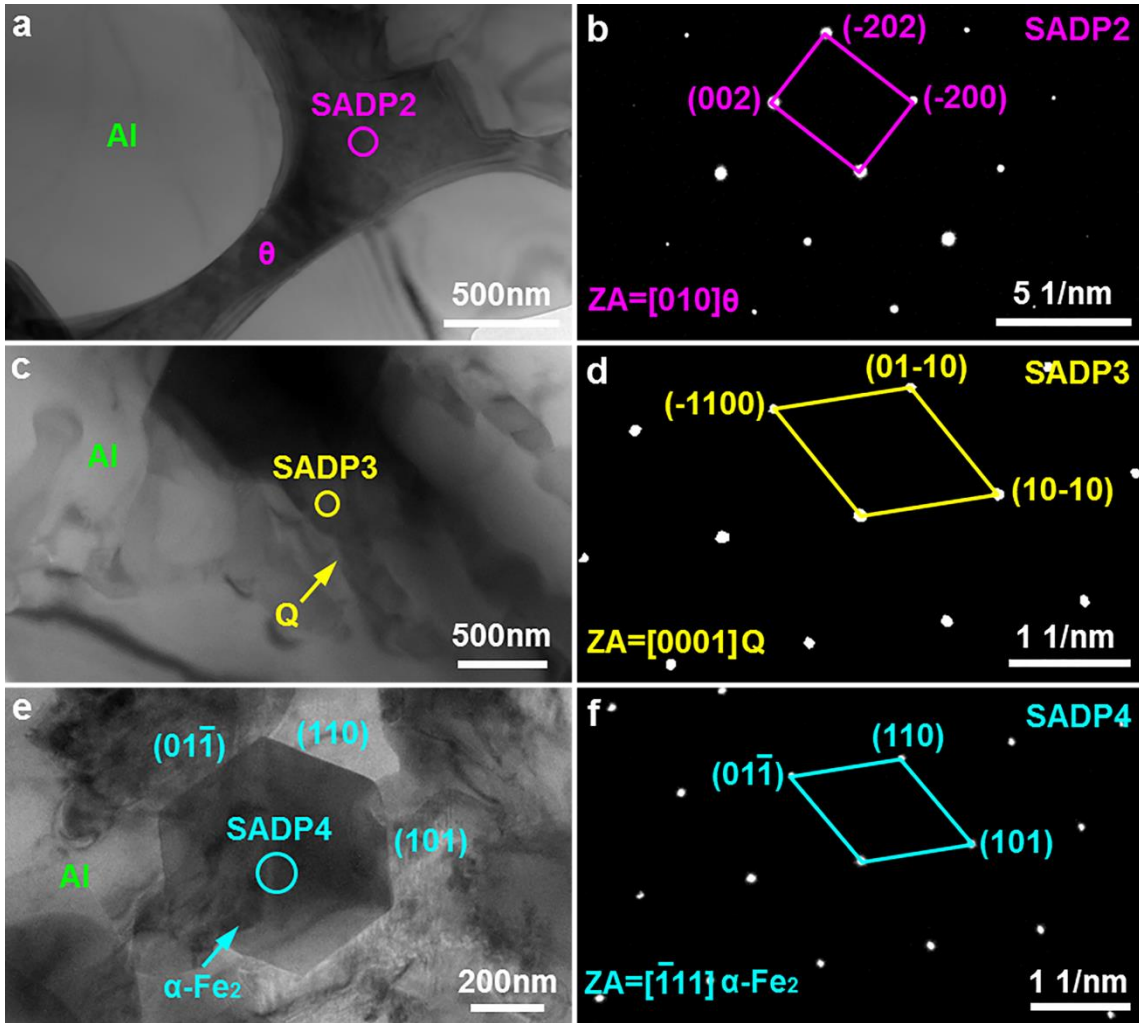


Fig. 4. TEM verification of the intermetallic compounds in the as-cast AlSi9Cu2Mg alloy. (a) TEM micrograph and (b) SADP of the θ compound, (c) TEM micrograph and (d) SADP of the Q compound, (e) TEM micrograph and (f) SADP of the α -Fe compound.

According to the (110) interplanar distance shown in Fig. 4f, the lattice constant of the α -Fe compound in the alloy was identified as 1.2702 nm, and the obtained lattice constant also fits well with the disclosed lattice constant of the α -Fe compound elsewhere [32]. The Mn/Fe ratio affects the formation of Fe-rich compound [33], and the Fe-rich compound formed in the present alloy with a high Mn/Fe ratio of 3:1 was similar to that in AlMg5Si2Mn0.7Fe1.1 [32] die-cast alloy with a low Mn/Fe ratio of 0.64:1.

3.1.2.4. Titanium diboride nanoparticles in die-cast alloys

Figs. 5 a and b show the TEM images of the as-cast AlSi9Cu2Mg alloy with the addition of 1.5wt.% TiB₂ nanoparticles, and most of the TiB₂ nanoparticles distribute at the grain boundaries (GB). Fig. 5c presents the SADP of the nanoparticle in Fig. 5b, and it verifies that

the nanoparticle is TiB_2 . Figs. 5d shows the TEM image of the as-cast $\text{AlSi}_9\text{Cu}_2\text{Mg}$ alloy with the addition of 3.0wt.% TiB_2 nanoparticles, and the majority of TiB_2 nanoparticles locate at the GB as well, while the quantity of TiB_2 nanoparticles in the GB is obviously increased. Li et al. [34] also noticed the presence of TiB_2 nanoparticles at the GB during the 3D printing of an Al-10Si-0.3Mg alloy.

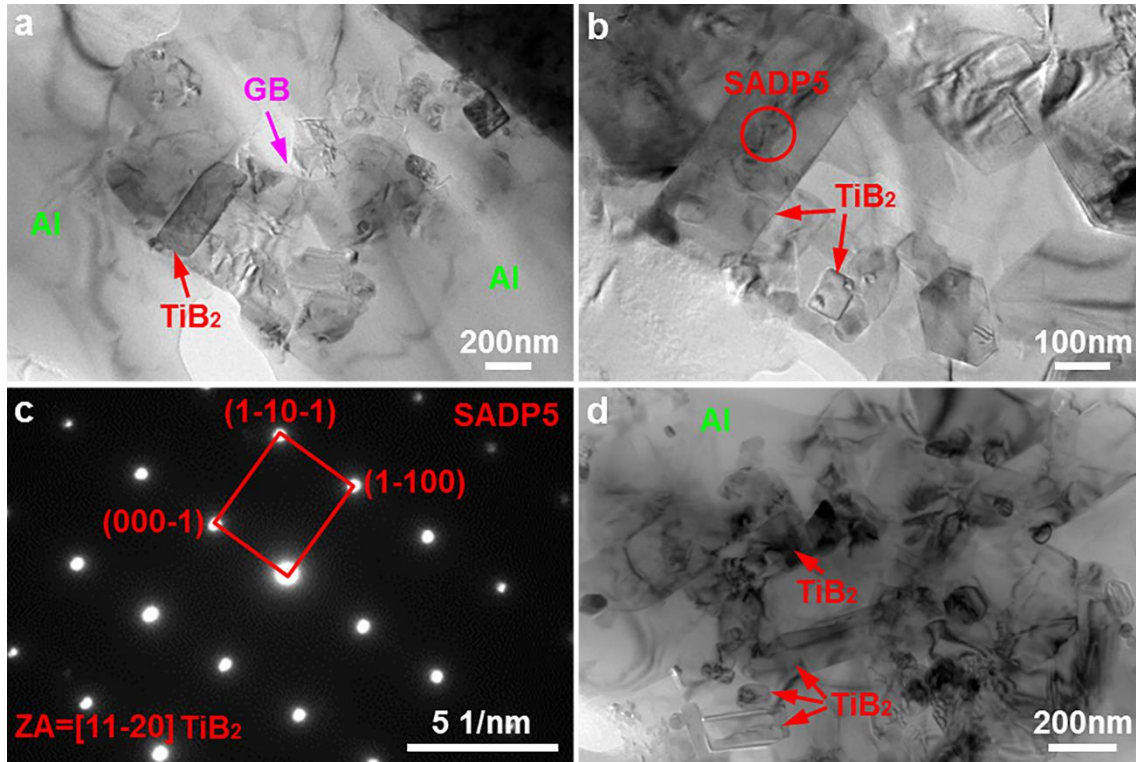


Fig. 5. TEM images of the TiB_2 nanoparticles in the as-cast $\text{AlSi}_9\text{Cu}_2\text{Mg}$ alloy. (a,b) TEM micrograph and (c) SADP of the TiB_2 nanoparticles in the alloy with the addition of 1.5wt.% TiB_2 nanoparticles. (d) TEM micrograph of the TiB_2 nanoparticles in the alloy containing 3.0wt.% TiB_2 nanoparticles.

3.1.2.5. XRD analysis results

Fig. 6 displays the XRD analysis results of the as-cast $\text{AlSi}_9\text{Cu}_2\text{Mg}$ alloy with the addition of 3.0wt.% TiB_2 nanoparticles. The peaks of Al, Si, Q, θ , $\alpha\text{-Fe}$ ($\text{Al}_{15}(\text{Fe},\text{Mn})_3\text{Si}_2$) and TiB_2 phases were found in the XRD pattern, which agrees with the results from SEM and TEM analysis. No peaks of the other phases such as AlB_2 and Al_3Ti were found in the XRD pattern of the alloy, and this indicates that the TiB_2 nanoparticles might not react with Al melt during casting. The TEM analysis result in Fig. 5 shows the sharp interface between the TiB_2 nanoparticles and the Al matrix, which also demonstrates that the TiB_2 nanoparticles might

not react with Al melt during casting. However, nanoparticles such as AlB_2 were reported [35] reacting with the solute atom Ti under the environment of Al melt and transforming into TiB_2 nanoparticles, as TiB_2 is more stable than AlB_2 under Ti-containing Al melt, and this might be the reason that TiB_2 nanoparticles did not react with Al melt here.

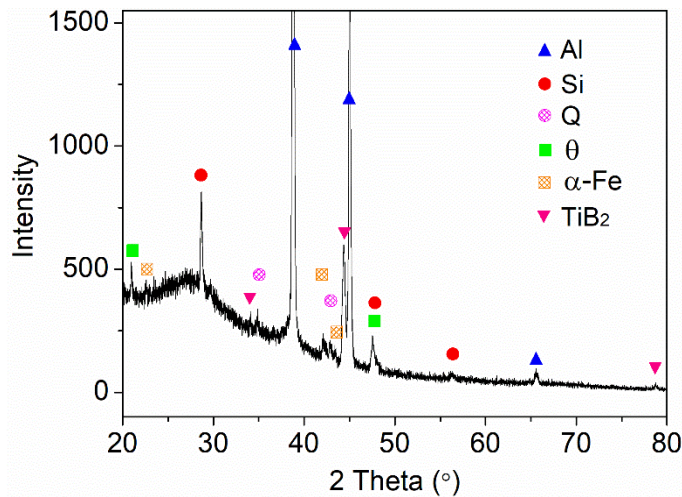


Fig. 6. XRD analysis of the as-cast AlSi9Cu2Mg alloy with 3.0wt.% TiB_2 nanoparticles.

3.2. Tensile performance

The tensile performance measured from the as-cast AlSi9Cu2Mg die-cast alloys with and without nanoparticles is shown in Fig. 7. The addition of TiB_2 nanoparticles could strengthen the AlSi9Cu2Mg die-cast alloy, and the tensile performance meets the trade-off of strength and ductility. The alloy without TiB_2 nanoparticles have the YS of 191 ± 2 MPa, UTS of 370 ± 5 MPa and EI of 7.9 ± 1.0 %. Meanwhile, the alloy containing 1.5wt.% TiB_2 nanoparticles shows the YS of 210 ± 2 MPa, UTS of 381 ± 6 MPa and EI of 6.6 ± 1.0 %. The alloy with 3.0wt.% TiB_2 nanoparticles demonstrates the YS of 233 ± 3 MPa, UTS of 398 ± 7 MPa and EI of 4.8 ± 0.7 %. Although the elongation is significantly reduced, it is still within the industrially acceptable level, by which the minimum elongation from round standard bar is 4% and the corresponding minimum elongation from casting body will be $>1.5\%$ by experience estimation. It is known that gas porosities are inevitably included in high pressure die castings due to the entrapment of gas during high speed injection [6]. Gas porosities have more significant effect on EI than YS and UTS [8,11], which results in the larger error bars on EI than that of YS and UTS in Fig. 7b. From Figs. 7c and d, the as-cast AlSi9Cu2Mg alloy with 3.0wt.% TiB_2 nanoparticles shows a minimum of 23 % improvement in YS and a minimum of 20 % enhancement in UTS. When comparing with the data from the existing die-

cast alloys [12–17], it is seen a significant improvement in yield strength and UTS, which is important in lightweight structures.

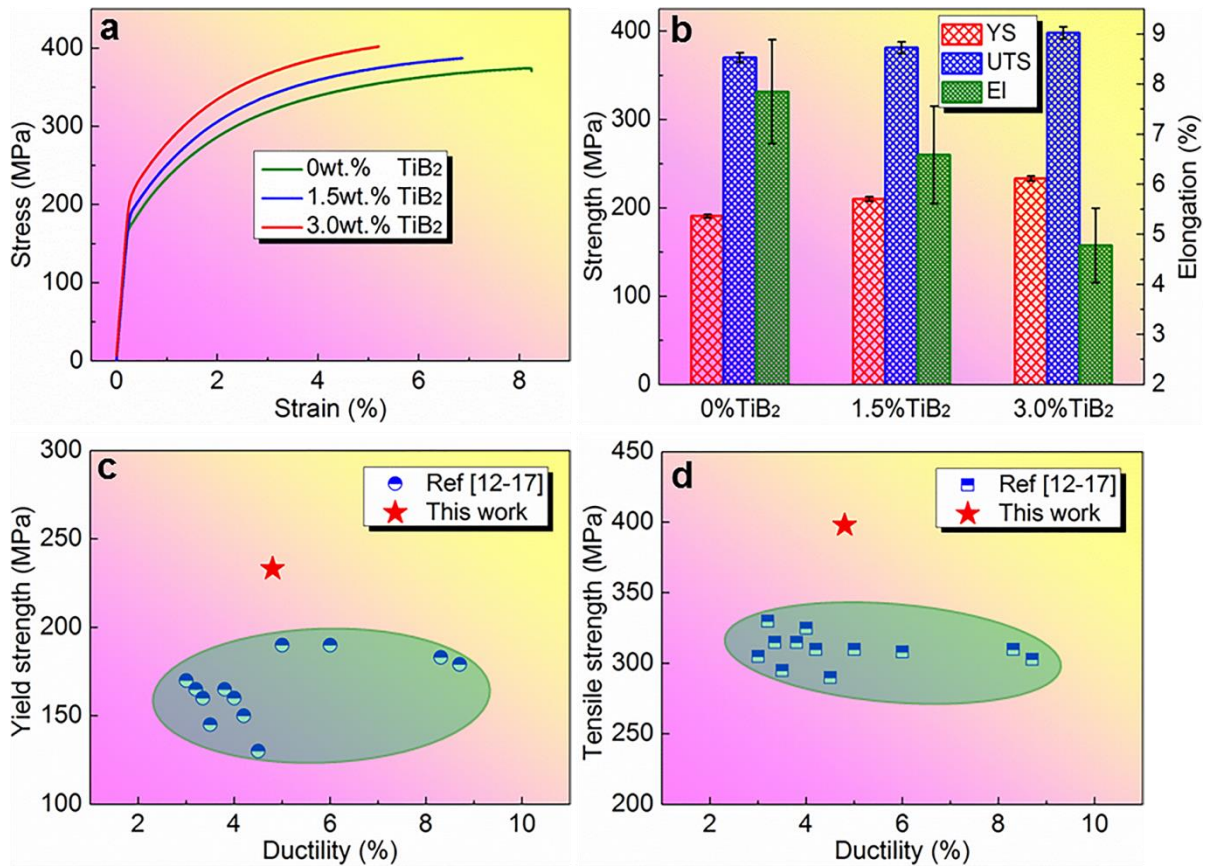


Fig. 7. Tensile performance of the as-cast AlSi9Cu2Mg alloys with different amount of TiB₂ nanoparticles. (a) Representative curves of the tensile test, (b) mean values of the tensile performance, (c,d) comparison of the tensile performance of the AlSi9Cu2Mg die-cast alloy containing 3.0wt.% TiB₂ nanoparticles with that of the existing die-cast Al alloys [12–17].

4. Discussion

4.1. Strengthening mechanism

4.1.1. Refinement of primary α -Al phase

The EBSD analysis results in Fig. 8 show the variation of grain size of α -Al phase in the as-cast AlSi9Cu2Mg alloys with the addition of TiB₂ nanoparticles. Fig. 8a shows the inverse pole figure (IPF) of the as-cast alloy without TiB₂ nanoparticles. Fig. 8b displays the statistical distribution of primary α -Al phase in Fig. 8a. The mean diameter of α -Al phase in the alloy was measured as 18.1 μ m. Fig. 8c presents the IPF of the alloy with 3.0wt.% TiB₂ nanoparticles, and Fig. 8d displays the statistical distribution of the α -Al phase in Fig. 8c.

The mean diameter of α -Al phase in the alloy 3.0wt.% TiB₂ nanoparticles was refined by 65 % to 6.4 μm . Similarly, the mean diameter of the α -Al phase in the alloy with 1.5wt.% TiB₂ nanoparticles was refined by 39 % to 11.1 μm . In addition to grain refinement, it was found that the columnar crystals nearly disappeared after adding TiB₂, and the equiaxed grains are dominant in the microstructure of the alloy reinforced by TiB₂. Furthermore, the α -Al grains and eutectic Si phase are more randomly oriented after the addition of TiB₂ in the alloys. The decrease of columnar crystals and orientation was also reported in the additive manufactured Al-Si cast alloys after adding nanoparticles [34,36]. The TiB₂ nanoparticles are excellent heterogeneous nucleation sites of Al [37]. Meanwhile, the presence of nanoparticles in the alloy melts is capable of suppressing the grain growth [38]. These could be the possible reasons for refining the α -Al phase in the AlSi9Cu2Mg die-cast alloys with different amount of nanoparticles. It needs to be emphasized that TiB₂ is normally recognised as not able to refine primary α -Al phase. However, the alloy itself contains some Ti or B in the melts. Therefore, the effect of grain refinement is still effective even only TiB₂ particles were added into the melt during experiments. It also should be mentioned that Si has a poisoning effect on TiB₂, which restrains the effectiveness of TiB₂ on the grain refinement of hypoeutectic cast Al-Si alloys with a Si content of over 4wt.%. In the past, the common belief was that silicide compounds especially Ti-Si compounds coated on TiB₂ particles [39] and resulted in the poisoning effect. However, the latest report [40] shows that Si atoms can segregate at the interface between TiB₂ and aluminium, and disturb the formation of TiAl₃ two-dimensional compound (2DC) that is critical for triggering the nucleation of α -Al on TiB₂ for grain refinement. The prevention of forming TiAl₃ compounds is the possible reason for Si poisoning in grain refinement.

In accordance with the well accepted Hall-Petch theory [41], the YS (σ_{ys}) of a material is inversely proportional to the square root of the grain diameter (d) of the phase in the material, as shown in Eq. (1).

$$\sigma_{ys} = \sigma_c + \frac{k}{\sqrt{d}} \quad (1)$$

Where σ_c is the stress constant, i.e., the critical stress for the activation of the shift of the dislocation in the material, and k is the enhancement factor for the YS of the material.

Therefore, the refinement of primary α -Al phase can result in the improvement of YS of the studied alloy. Based on Eq. (1), the increase of yield strength in the AlSi9Cu2Mg alloy with

1.5wt.% TiB₂ nanoparticles is ~4 MPa, and that in the alloy with 3.0wt.% TiB₂ nanoparticles is ~10 MPa.

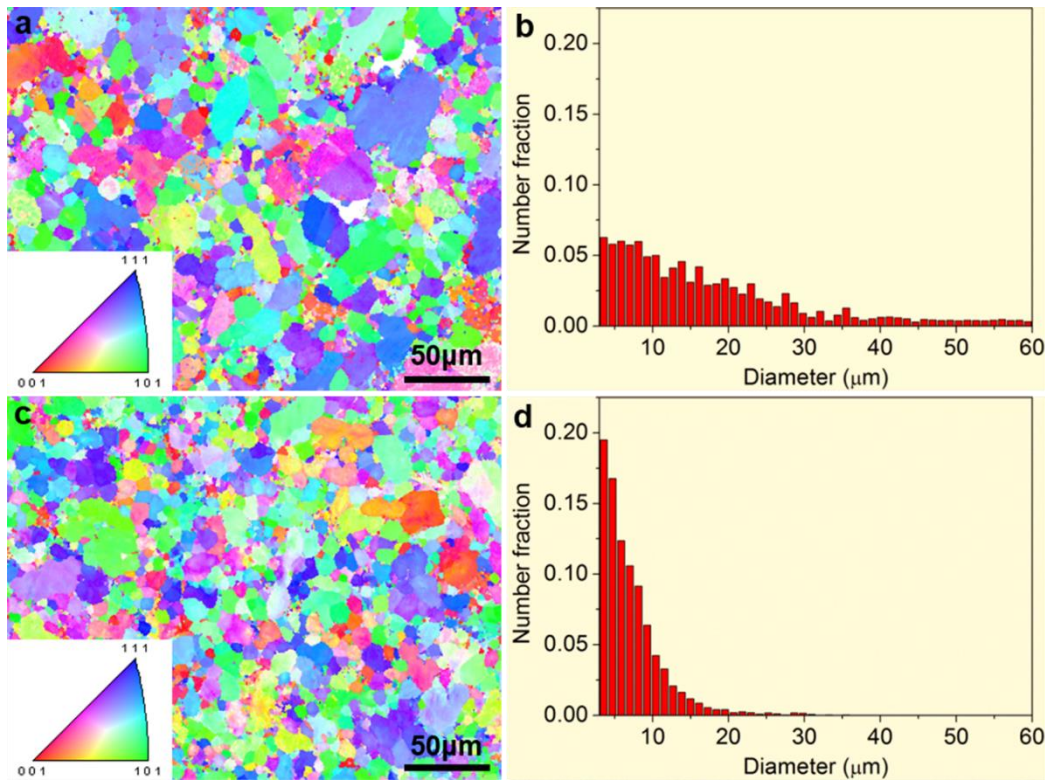


Fig. 8. EBSD analysis of the as-cast AlSi9Cu2Mg alloys. (a) Inverse pole figure and (b) statistical distribution of primary α -Al phase in the alloy without TiB₂ nanoparticles, (c) Inverse pole figure and (d) statistical distribution of primary α -Al phase in the alloy with 3.0wt.% TiB₂ nanoparticles.

4.1.2. Nanoparticle and interface

Fig. 9 displays the interface between the TiB₂ nanoparticle and the Al matrix in the as-cast AlSi9Cu2Mg alloy with 3.0wt.% TiB₂ nanoparticles, which was observed at the zone axis of [11-20] of the TiB₂ nanoparticle. Fig. 9a shows the TEM morphology of the observing TiB₂ nanoparticle, and Fig. 9b presents the enlarged morphology of the TiB₂ nanoparticle in Fig. 9a. Fig. 9c shows the HRTEM micrograph of the interfacial features between the observed TiB₂ nanoparticle and the surrounding Al matrix in Figs. 9 a and b. The (11-1) lattice face of the Al matrix was found parallel to the (0001) lattice face of TiB₂ nanoparticle (Fig. 9c), which indicates the existence of coherent interface between the Al matrix and the TiB₂ nanoparticle. The fast Fourier transform (FFT) pattern of the observed interface clearly

confirms that the TiB_2 nanoparticle has coherent interface with the surrounding Al matrix in the present studied alloy.

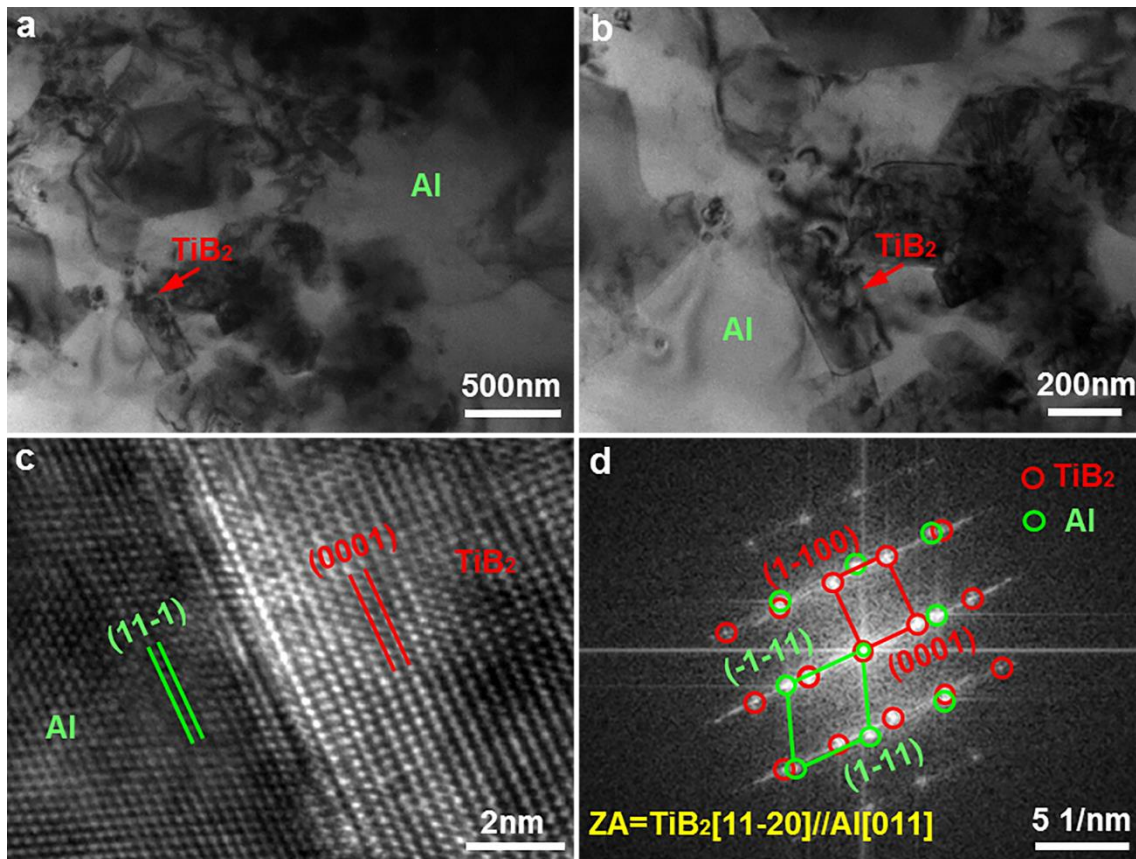


Fig. 9. TEM images showing the interface between the TiB_2 nanoparticle and the Al matrix in the as-cast AlSi9Cu2Mg alloy along the $[11-20]$ zone axis of the TiB_2 nanoparticle. (a,b) TEM micrographs of TiB_2 particles, (c) high resolution micrograph and (d) FFT of the interface between Al- TiB_2 phases.

As mentioned before, the yield strength of as-cast AlSi9Cu2Mg alloys with 1.5wt.% and 3.0wt.% TiB_2 nanoparticles are improved by 19 MPa and 42 MPa, respectively, when compared with the one without TiB_2 nanoparticles. The contribution of grain refinement is 4 MPa for the alloy with 1.5wt.% TiB_2 nanoparticles and 10 MPa for the alloy with 3.0wt.% TiB_2 nanoparticles. The contribution from the addition of nanoparticles is 15 MPa for the alloy with 1.5wt.% TiB_2 nanoparticles and 32 MPa the alloy with 3.0wt.% TiB_2 nanoparticles. Clearly, the strengthening from the addition of TiB_2 nanoparticles is more effective than grain refinement. Usually the agglomeration is a significant concern for adding particles into Al melt. However, the in-situ creation of nanoparticles is beneficial for diminishing the

agglomeration. More importantly, the high-speed fluid shear generated during the die filling of HPDC was reported helpful for the uniform dispersion of particles [27]. Therefore, the particles in the present study are not prone to agglomeration under HPDC. Therefore, the ductility of the die cast samples is still acceptable when TiB₂ particles is at a level of 3.0 wt.%.

4.2. Effect on fracture

Fig. 10 present the tensile fracture of the AlSi9Cu2Mg die-cast alloy with different amount of TiB₂ nanoparticles. The α -Al phase, the eutectic Si phase, TiB₂ particles and the compounds of θ , α -Fe and Q were recognized on the fractured surface, which conforms with the SEM observation in Fig. 3. The α -Al phase on the fractured surface is shown as dimples due to the ductile characteristic. Cracks are present in the silicon phase resulting from its relatively brittle nature [48–53], while seldom cracks were observed from the θ , α -Fe and Q compounds, which demonstrates that the main resources of cracks are silicon phase in the die-cast AlSi9Cu2Mg alloy without TiB₂ nanoparticles. In the alloy with TiB₂ nanoparticles, the TiB₂ nanoparticles are present on the fractured surface in addition to the α -Al dimples, Si phase and θ , α -Fe and Q compounds. Cracks are mainly observed from the Q and α -Fe compounds, and hardly find from the Si phase and θ compound. The EDS analysis results of the silicon phase and the θ , α -Fe, and Q compounds on the fractured surface are shown in Fig. 2S in the supplementary material.

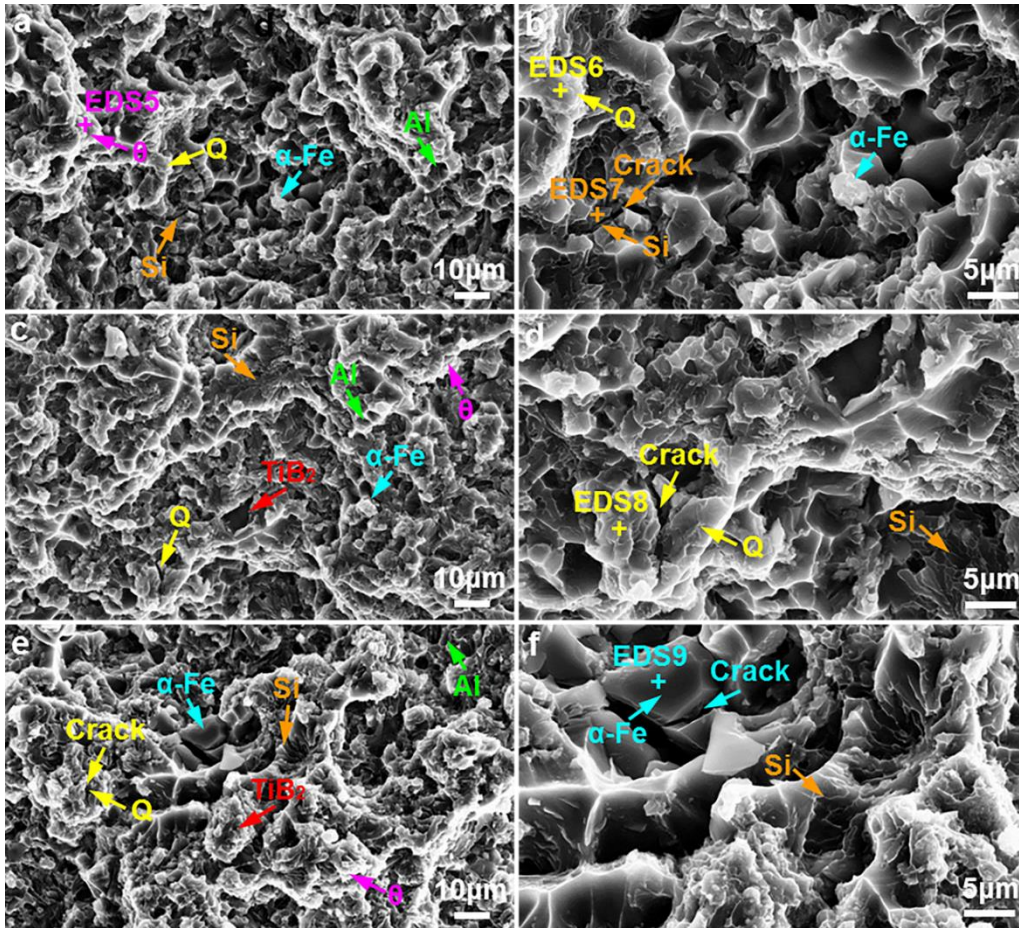


Fig. 10. SEM images showing the fractured surface of as-cast AlSi9Cu2Mg alloy, (a,b) without TiB₂ nanoparticles, (c,d) with 1.5wt.% TiB₂ nanoparticles, (e,f) with 3.0wt.% TiB₂ nanoparticles.

According to the fracture analysis in Fig. 10, the addition of TiB₂ nanoparticles affects the fracture mechanism in the die-cast AlSi9Cu2Mg alloy, and the die-cast alloy breaks more easily from the Q and α-Fe compounds than the silicon phase, after the addition of TiB₂ nanoparticles. The deformation ability of different phases themselves might not change much after the addition of TiB₂ nanoparticles in the present AlSi9Cu2Mg die-cast alloy. However, distribution of Si phase may be varied because of the addition of TiB₂ particles. This can be the possible reasons for the difference of fracture mechanism.

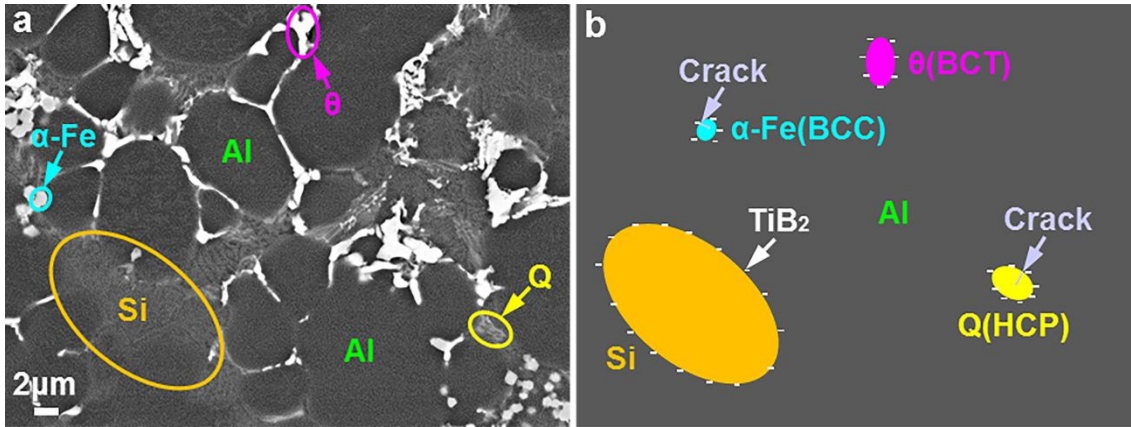


Fig. 11. Breaking mechanism of the as-cast AlSi9Cu2Mg alloys, (a) detail of the multiple phases in the die-cast alloys under SEM observation, (b) schematic diagram showing the fracturing mechanism.

Fig. 11a displays the sizes of the silicon phase and the compounds of θ , α -Fe and Q in the as-cast AlSi9Cu2Mg alloys under backscattered SEM observation. The size of silicon phase is much larger than that of the θ , α -Fe and Q compounds. Fig. 11b presents the schematic diagram showing the relative sizes of different phases in the AlSi9Cu2Mg die-cast alloys and the possible mechanism for breakage. The silicon phase is breakable [48–53], however, the size of the silicon phase is significantly larger than that of the TiB₂ nanoparticles, and cracks were not easy to form in the large silicon phase when interacted with the small hard TiB₂ nanoparticles after loading. The size of θ compound is comparable to the size of TiB₂ nanoparticles, however, θ compound is ductile and easy to deform under loading, so cracks hardly form in θ compound. The sizes of Q and α -Fe compounds are also comparable to the TiB₂ nanoparticles, but these two phases are hard to deform, so Q and α -Fe compounds were more easily to crack when interacted with the small hard TiB₂ nanoparticles after loading, and cracks formed in Q and α -Fe compounds, while cracks hardly formed in the silicon phase as Q and α -Fe compounds cracked in advance. Thus, the addition of the TiB₂ nanoparticles promote the crack of the Q and Fe compounds instead of the crack of the eutectic silicon phase in the present as-cast AlSi9Cu2Mg die-cast alloys.

5. Conclusions

High strength die-cast AlSi9Cu2Mg alloy was achieved under as-cast condition through the addition of TiB₂ nanoparticles. The main results are summarized as below:

(1) The die-cast AlSi9Cu2Mg alloy with 3.0wt.% TiB₂ nanoparticles offers the yield strength of 233±3 MPa, ultimate tensile strength of 398±7 MPa, and elongation of 4.8±0.7 % under as-cast condition showing an improvement of 23 % in comparison with the alloy without TiB₂ nanoparticles.

(2) The main intermetallic compounds in the as-cast AlSi9Cu2Mg alloy are identified as θ -Al₂Cu and Q-Al₅Cu₂Mg₈Si₆ phases. The Fe-rich compound formed in the as-cast AlSi9Cu2Mg alloy with a Mn/Fe ratio of 3:1 was determined as the BCC α -Al₁₅(Fe,Mn)₃Si₂ phase with a lattice parameter of $a = 1.2702$ nm, and have a highly faceted morphology with {110} surface termination.

(3) The primary α -Al phase in the die-cast AlSi9Cu2Mg alloy with 3.0wt.% TiB₂ nanoparticles is refined to 6.4 μ m from 18.1 μ m in the alloy without TiB₂ addition. The TiB₂ nanoparticles have coherent interface with Al matrix, in which the (11-1) lattice face of Al is parallel to the (0001) lattice face of TiB₂.

(4) The as-cast yield strength of the die-cast AlSi9Cu2Mg alloy is strengthened by 42 MPa with the addition of 3.0wt.% TiB₂ nanoparticles. The contribution of the strengthening by nanoparticles is 32 MPa and that by refining the primary α -Al phase is 10 MPa.

(5) The addition of TiB₂ nanoparticles affects the fracture of as-cast AlSi9Cu2Mg alloy. The cracks are formed from the Q-Al₅Cu₂Mg₈Si₆ and α -Al₁₅(Fe,Mn)₃Si₂ phases, rather than from the eutectic silicon phase in the TiB₂ enhanced AlSi9Cu2Mg alloy under as-cast condition.

Acknowledgements

The study is funded by the Innovate UK project. Jon Gadd from BCAST is greatly appreciated for the professional assistance of the high pressure die casting experiments.

Declaration of competing interest

The authors declare no conflict of interest.

CRedit authorship contribution statement

X.X. Dong: Conceptualization, Investigation, Data curation, Formal analysis, Writing & Revision. **H. Youssef:** Experiments, Investigation, Formal analysis. **X.Z. Zhu:** XRD analysis,

Revision. **Y.J. Zhang:** Investigation, Material preparation. **S.H. Wang:** Investigation, Revision. **S. Ji:** Funding acquisition, Conceptualization, Supervision, Review & Revision.

References

- [1] X.X. Dong, X.S. Huang, L.H. Liu, L.J. He, P.J. Li, A liquid aluminum alloy electromagnetic transport process for high pressure die casting, *J. Mater. Process. Technol.* 234 (2016) 217–227.
- [2] X.X. Dong, G.B. Mi, L.J. He, P.J. Li, 3D simulation of plane induction electromagnetic pump for the supply of liquid Al–Si alloys during casting, *J. Mater. Process. Technol.* 213 (2013) 1426–1432.
- [3] L.H. Liu, T. Zhang, Z.Y. Liu, C.Y. Yu, X.X. Dong, L.J. He, K. Gao, X.G. Zhu, W.H. Li, C.Y. Wang, P.J. Li, L.C. Zhang, L. Li, Near-net forming complex shaped Zr-based bulk metallic glasses by high pressure die casting, *Materials* 11 (2018) 2338.
- [4] X.X. Dong, L.J. He, X.S. Huang, P.J. Li, Coupling analysis of the electromagnetic transport of liquid aluminum alloy during casting, *J. Mater. Process. Technol.* 222 (2015) 197–205.
- [5] X.X. Dong, H.L. Yang, X.Z. Zhu, S. Ji, High strength and ductility aluminium alloy processed by high pressure die casting, *J. Alloys Compd.* 773 (2019) 86–96.
- [6] L.H. Wang, P. Turnley, G. Savage, Gas content in high pressure die castings, *J. Mater. Process. Technol.* 211 (2011) 1510–1515.
- [7] X.X. Dong, L.J. He, X.S. Huang, P.J. Li, Effect of electromagnetic transport process on the improvement of hydrogen porosity in A380 aluminum alloy, *Int. J. Hydrogen Energy* 40 (2015) 9287–9297.
- [8] X.Z. Zhu, H.L. Yang, X.X. Dong, S.X. Ji, The effects of varying Mg and Si levels on the microstructural inhomogeneity and eutectic Mg₂Si morphology in die-cast Al–Mg–Si alloys, *J. Mater. Sci.* 54 (2019) 5773–5787.
- [9] X.X. Dong, X.Z. Zhu, S. Ji, Effect of super vacuum assisted high pressure die casting on the repeatability of mechanical properties of Al–Si–Mg–Mn die-cast alloys, *J. Mater. Process. Technol.* 266 (2019) 105–113.
- [10] X.X. Dong, H. Youssef, Y.J. Zhang, S.H. Wang, S.X. Ji, High performance Al/TiB₂ composites fabricated by nanoparticle reinforcement and cutting-edge super vacuum assisted die casting process, *Compos. Part B Eng.* 177 (2019) 107453.

- [11] X.X. Dong, H. Youssef, Y.J. Zhang, H.L. Yang, S.H. Wang, S.X. Ji, Advanced heat treated die-cast aluminium composites fabricated by TiB₂ nanoparticle implantation, *Mater. Des.* 186 (2020) 108372.
- [12] S. Ji, F. Yan, Z. Fan, Development of a high strength Al–Mg₂Si–Mg–Zn based alloy for high pressure die casting, *Mater. Sci. Eng. A* 626 (2015) 165–174.
- [13] Y. Zhang, J.B. Patel, J. Lazaro-Nebreda, Z. Fan, Improved defect control and mechanical property variation in high-pressure die casting of A380 alloy by high shear melt conditioning, *JOM* 70 (2018) 2726–2730.
- [14] Z.Q. Hu, L. Wan, S.S. Wu, H. Wu, X.Q. Liu, Microstructure and mechanical properties of high strength die-casting Al–Mg–Si–Mn alloy, *Mater. Des.* 46 (2013) 451–456.
- [15] L.Y. Yuan, L.M. Peng, J.Y. Han, B.L. Liu, Y.J. Wu, J. Chen, Effect of Cu addition on microstructures and tensile properties of high-pressure die-casting Al-5.5Mg-0.7Mn alloy, *J. Mater. Sci. Technol.* 35 (2019) 1017–1026.
- [16] P. Zhang, Z.M. Li, B.L. Liu, W.J. Ding, Effect of chemical compositions on tensile behaviors of high pressure die-casting alloys Al-10Si-yCu-xMn-zFe, *Mater. Sci. Eng. A* 661 (2016) 198–210.
- [17] X.Z. Zhu, P. Blake, K. Dou, S. Ji, Strengthening die-cast Al-Mg and Al-Mg-Mn alloys with Fe as a beneficial element, *Mater. Sci. Eng. A* 732 (2018) 240–250.
- [18] D.J. Lloyd, Particle reinforced aluminium and magnesium matrix composites, *Int. Mater. Rev.* 39 (1994) 1–23.
- [19] X.D. Sui, C.P. Luo, Z.X. Luo, L.Z. Ouyang, The fabrication and properties of particle reinforced cast metal matrix composites, *J. Mater. Process. Technol.* 63 (1997) 426–431.
- [20] L.Y. Chen, J.Q. Xu, H. Choi, M. Pozuelo, X.L. Ma, S. Bhowmick, J.M. Yang, S. Mathaudhu, X.C. Li, Processing and properties of magnesium containing a dense uniform dispersion of nanoparticles, *Nature* 528 (2015) 539–543.
- [21] Y.W. Shen, X.F. Li, T.R. Hong, J.W. Geng, H.W. Wang, Effects of TiB₂ particles on microstructure and mechanical properties of an *in-situ* TiB₂-Al-Cu-Li matrix composite, *Mater. Sci. Eng. A* 655 (2016) 265–268.
- [22] S.A. Sajjadi, H.R. Ezatpour, H. Beygi, Microstructure and mechanical properties of Al–Al₂O₃ micro and nano composites fabricated by stir casting, *Mater. Sci. Eng. A* 528 (2011) 8765–8771.
- [23] Z.Y. Ma, Y.L. Li, Y. Liang, F. Zheng, J. Bi, S.C. Tjong, Nanometric Si₃N₄ particulate-reinforced aluminum composite, *Mater. Sci. Eng. A* 219 (1996) 229–231.

- [24] K. Kalaiselvan, N. Murugan, S. Parameswaran, Production and characterization of AA6061–B₄C stir cast composite, *Mater. Des.* 32 (2011) 4004–4009.
- [25] S. Jerome, B. Ravisankar, P.K. Mahato, S. Natarajan, Synthesis and evaluation of mechanical and high temperature tribological properties of in-situ Al–TiC composites, *Tribol. Int.* 43 (2010) 2029–2036.
- [26] S.M.S. Reihani, Processing of squeeze cast Al6061-30vol% SiC composites and their characterization, *Mater. Des.* 27 (2006) 216–222.
- [27] Q.Y. Hu, H.D. Zhao, F.D. Li, Microstructures and properties of SiC particles reinforced aluminum–matrix composites fabricated by vacuum-assisted high pressure die casting, *Mater. Sci. Eng. A* 680 (2017) 270–277.
- [28] S. Lakshmi, L. Lu, M. Gupta, In situ preparation of TiB₂ reinforced Al based composites, *J. Mater. Process. Technol.* 73 (1998) 160–166.
- [29] A. Abdel-Hamid, S. Hamar-Thibault, R. Hamar, Crystal morphology of the compound TiB₂, *J. Cryst. Growth* 71 (1985) 744–750.
- [30] Y. Tang, Z. Chen, A. Borbély, G. Ji, S.Y. Zhong, D. Schryvers, V. Ji, H.W. Wang, Quantitative study of particle size distribution in an in-situ grown Al–TiB₂ composite by synchrotron X-ray diffraction and electron microscopy, *Mater. Charact.* 102 (2015) 131–136.
- [31] W.C. Yang, S. Ji, X.R. Zhou, I. Stone, G. Scamans, G.E. Thompson, Z. Fan, Heterogeneous nucleation of α -Al grain on primary α -AlFeMnSi intermetallic investigated using 3D SEM ultramicrotomy and HRTEM, *Metall. Mater. Trans. A* 45 (2014) 3971–3980.
- [32] Z.P. Que, Y. Wang, Z. Fan, Formation of the Fe-Containing Intermetallic Compounds during Solidification of Al-5Mg-2Si-0.7Mn-1.1Fe Alloy, *Metall. Mater. Trans. A* 49 (2018) 2173–2181.
- [33] Q. Cai, C.L. Mendis, I.T.H. Chang, Z. Fan, Effect of short T6 heat treatment on the microstructure and the mechanical properties of newly developed die-cast Al–Si–Mg–Mn alloys, *Mater. Sci. Eng. A* 788 (2020) 139610.
- [34] X.P. Li, G. Ji, Z. Chen, A. Addad, Y. Wu, H.W. Wang, J. Vleugels, J. Van Humbeeck, J.P. Kruth, Selective laser melting of nano-TiB₂ decorated AlSi10Mg alloy with high fracture strength and ductility, *Acta Mater.* 129 (2017) 183–193.
- [35] Y. Birol, Performance of AlTi5B1, AlTi3B3 and AlB3 master alloys in refining grain structure of aluminium foundry alloys, *Mater. Sci. Technol.* 28 (2012) 481–486.

- [36] C. Gao, W. Wu, J. Shi, Z. Xiao, A.H. Akbarzadeh, Simultaneous enhancement of strength, ductility, and hardness of TiN/AlSi10Mg nanocomposites via selective laser melting, *Addit. Manuf.* 34 (2020) 101378.
- [37] Z. Fan, Y. Wang, Y. Zhang, T. Qin, X.R. Zhou, G.E. Thompson, T. Pennycook, T. Hashimoto, Grain refining mechanism in the Al/Al–Ti–B system, *Acta Mater.* 84 (2015) 292–304.
- [38] C.Z. Cao, G.C. Yao, L. Jiang, M. Sokoluk, X. Wang, J. Cistons, A. Javadi, Z.Y. Guan, I. De Rosa, W.G. Xie, E.J. Lavernia, J.M. Schoenung, X.C. Li, Bulk ultrafine grained/nanocrystalline metals via slow cooling, *Sci. Adv.* 5 (2019) eaaw2398.
- [39] P.S. Mohanty, J.E. Gruzleski, Grain refinement mechanisms of hypoeutectic Al–Si alloys, *Acta Metall. Mater.* 44 (1996) 3749–3760.
- [40] Y. Li, B. Hu, B. Liu, A.M. Nie, Q.F. Gu, J.F. Wang, Q. Li, Insight into Si poisoning on grain refinement of Al–Si/Al–5Ti–B system, *Acta Mater.* 187 (2020) 51–65.
- [41] I. Gutierrez-Urrutia, M.A. Muñoz-Morris, D.G. Morris, Contribution of microstructural parameters to strengthening in an ultrafine-grained Al–7% Si alloy processed by severe deformation, *Acta Mater.* 55 (2007) 1319–1330.
- [42] S. Gorsse, D.B. Miracle, Mechanical properties of Ti–6Al–4V/TiB composites with randomly oriented and aligned TiB reinforcements, *Acta Mater.* 51 (2003) 2427–2442.
- [43] L.J. Huang, L. Geng, A.B. Li, F.Y. Yang, H.X. Peng, In situ TiBw/Ti–6Al–4V composites with novel reinforcement architecture fabricated by reaction hot pressing, *Scr. Mater.* 60 (2009) 996–999.
- [44] L.G. Huang, F.T. Kong, Y.Y. Chen, S.L. Xiao, L.J. Xu, Effects of trace TiB₂ on microstructure in cast titanium alloys, *Int. J. Cast Metal. Res.* 25 (2012) 358–363.
- [45] Y. Jiao, L.J. Huang, T.B. Duan, S.L. Wei, B. Kaveendran, Controllable two-scale network architecture and enhanced mechanical properties of (Ti₅Si₃+TiBw)/Ti₆Al₄V composites, *Sci. Rep.* 6 (2016) 32991.
- [46] H.Y. Lu, D.L. Zhang, B. Gabbitas, F. Yang, S. Matthews, Synthesis of a TiBw/Ti₆Al₄V composite by powder compact extrusion using a blended powder mixture, *J. Alloys Compd.* 606 (2014) 262–268.
- [47] W.C. Zhang, Y.J. Feng, W.Z. Chen, J.L. Yang, Effects of heat treatment on the microstructure and mechanical properties of in situ inhomogeneous TiBw/Ti₆Al₄V composite fabricated by pre-sintering and canned powder extrusion, *J. Alloys Compd.* 693 (2017) 1116–1123.

- [48] X.X. Dong, Y.J. Zhang, S.X. Ji, Enhancement of mechanical properties in high silicon gravity cast AlSi9Mg alloy refined by Al₃Ti₃B master alloy, *Mater. Sci. Eng. A* 700 (2017) 291–300.
- [49] X.X. Dong, S.X. Ji, Si poisoning and promotion on the microstructure and mechanical properties of Al–Si–Mg cast alloys, *J. Mater. Sci.* 53 (2018) 7778–7792.
- [50] L.F. Li, S.X. Ji, Q. Zhu, Y. Wang, X.X. Dong, W.C. Yang, S. Midson, Y.L. Kang, Effect of Zn concentration on the microstructure and mechanical properties of Al–Mg–Si–Zn alloys processed by gravity die casting, *Metall. Mater. Trans. A* 49 (2018) 3247–3256.
- [51] X.X. Dong, L.J. He, G.B. Mi, P.J. Li, Dynamic investigation of the finite dissolution of silicon particles in aluminum melt with a lower dissolution limit, *Chin. Phys. B* 23 (2014) 110204.
- [52] X.X. Dong, Y.J. Zhang, S. Amirkhanlou, S.X. Ji, High performance gravity cast Al₉Si_{0.45}Mg_{0.4}Cu alloy inoculated with AlB₂ and TiB₂, *J. Mater. Process. Technol.* 252 (2018) 604–611.
- [53] X.X. Dong, S. Amirkhanlou, S.X. Ji, Formation of strength platform in cast Al–Si–Mg–Cu alloys, *Sci. Rep.* 9 (2019) 9582.
- [54] Z.D. Li, N. Limodin, A. Tandjaoui, P. Quaegebeur, P. Osmond, Influence of Sr, Fe and Mn content and casting process on the microstructures and mechanical properties of AlSi₇Cu₃ alloy, *Mater. Sci. Eng. A* 689 (2017) 286–297.